Evolution of Magnetic Oxygen States in Sr-Doped $LaCoO_3$

S. Medling,[1] Y. Lee,[2] H. Zheng,[3] J. F. Mitchell,[3] J. W. Freeland,[4] B. N. Harmon,[2] and F. Bridges[1]

[1]*Department of Physics, University of California, Santa Cruz, California 95064, USA*
[2]*Ames Laboratory and Iowa State University, Ames, Iowa 50011-3020, USA*
[3]*Materials Science Division, Argonne National Laboratory, 9700 Cass Avenue, Argonne, Illinois 60439, USA*
[4]*Advanced Photon Source, Argonne National Laboratory, 9700 Cass Avenue, Argonne, Illinois 60439, USA*

(Received 12 June 2012; published 9 October 2012)

Magnetism in $La_{1-x}Sr_xCoO_3$ as a function of doping is investigated with x-ray absorption spectroscopy and x-ray magnetic circular dicrhoism at the O K edge, and corresponding first principles electronic structure calculations. For small x, the spectra are consistent with the formation of ferromagnetic clusters occurring within a nonmagnetic insulating matrix. Sr-induced, magnetic O-hole states form just above E_F and grow with increasing Sr doping. Density functional calculations for $x = 0$ yield a nonmagnetic ground state with the observed rhombohedral distortion and indicates that doping introduces holes at the Fermi level in magnetic states with significant O $2p$ and Co t_{2g} character for the undistorted pseudocubic structure. Supercell calculations show stronger magnetism on oxygen atoms having more Sr neighbors.

DOI: 10.1103/PhysRevLett.109.157204 PACS numbers: 75.47.Lx, 71.55.Ht, 78.20.Fm, 78.70.Dm

Doping in complex oxides is a fundamental route for control of the many degrees of freedom. However, depending on the nature of the underlying ground state, the impact on the local electronic structure depends strongly on the balance between on-site energies and the bonding to oxygen [1,2]. For example, doping in the Mott regime directly changes the valence state of the transition metal ion (e.g., manganites) while doping in the extreme of the charge transfer regime (e.g., cuprates) results in formation of holes on the oxygen lattice. The case of cobaltites lies in the crossover region between these two extremes and a better understanding of this regime may finally answer the decades-old question of why magnetism in $La_{1-x}Sr_xCoO_3$ (LSCO) is so unusual.

$LaCoO_3$ is a nonmagnetic, small gap semiconductor at low T, but at increased temperature and particularly with Sr doping on the La sites, the material exhibits a wealth of unusual magnetic properties associated with Co sites acquiring a substantial magnetic moment ($\sim 1.3\,\mu_B$). For $x > 0.18$, the crystal becomes ferromagnetic (FM) and metallic [3–7]; see Fig. 5 of Ref. [7] for a phase diagram. With increasing x, the rhombohedral structural distortion gradually decreases and the crystal approaches the cubic perovskite structure [8].

Most studies of LSCO have used localized models, which assume that the dominant interactions are the crystal field splitting and the exchange interactions E_{ex}; these interactions split the Co $3d$ energy levels into narrow t_{2g} and e_g multiplets and also split the spin-up and spin-down states. Within such models, there is extensive debate about the spin states, with low spin ($S = 0$, $t_{2g}^6 e_g^0$) [9] at low T and a possible mixture of low spin and either an intermediate spin ($S = 1$, $t_{2g}^5 e_g^1$) [10] or a high spin state ($S = 2$, $t_{2g}^4 e_g^2$) at higher T or with Sr doping. However, we argue that this localized picture is not appropriate—the e_g states interact with O $2p$ states and are spread over a large energy range (10 eV), from low energy bonding states to high energy antibonding states.

In Co K-edge x-ray absorption near edge spectroscopy (XANES) studies [11,12] the Co K edge shifts ≤ 0.15 eV as x increases to 0.3, in stark contrast to other Co systems and many manganites, for which the edge shift is roughly 3 eV per valence unit [13–15]. Further, both diffraction studies [16,17] and extended x-ray absorption fine structure (EXAFS) results [12] show that the Co-O bond length is nearly independent of x for LSCO; consequently, the bond-valence sum model also indicates no change in Co valence, i.e., the $3d$ electron configuration remains close to d^6. This raises the question: Where do the Sr-induced holes go? We argued that a large fraction of the holes are on the O atoms [12], which can be directly probed at the oxygen K edge. Previous x-ray absorption spectroscopy (XAS) studies at the O K edge show an evolution with hole doping [18,19], but existing x-ray magnetic circular dichroism (XMCD) studies are limited [20,21]. Thus, to date there has been no systematic study of the low hole doping regime to follow the connection between local structure and changes in electronic and magnetic states.

Here, we present a detailed doping-dependent study of the oxygen hole states in LSCO single crystals, using polarization-dependent XAS to track the first O preedge peak (Co-O ligand hole states). It is clear that a magnetic state with a large O component forms with doping and the increase in O absorption is tied to a large fraction of the doped holes residing on the oxygen site. The strong XMCD shows directly that there is a nonzero orbital moment on oxygen (and correspondingly, a net O magnetic moment). The analysis shows the moment on oxygen is parallel to the Co moment and increases in magnitude with doping. To understand these results and determine the magnetic

structure of O, complementary theoretical studies have been carried out; they show that the $3d$ electron density of states (DOS) are spread over a large energy range, with significant e_g character for bonding states 6 eV below E_F. They also show that the (empty) O DOS just above the Fermi level increases with x, and that the O atoms develop a moment, with both spin and orbital components. Most important, the O atoms are no longer equivalent; their properties depend on the number of nearest Sr neighbors.

XMCD and XAS data for the O K edges were measured at the Advanced Photon Source beam line 4-ID-C. A superconducting magnet provided magnetic fields up to ± 5 T. The energy resolution was ~ 0.15 eV. Small single crystals were mounted on an electrode using Ag paste and scraped with a diamond file to remove surface contamination. The x-ray beam was oriented at 45° to the sample surface and the fluorescence detector was at 90° to the beam.

The XAS fluorescence data at the O K edge are shown in Fig. 1. A small constant background was subtracted from the XAS and then the data were normalized to 1 at energy 550 eV. Finally, the data were corrected for self-absorption following the method in the computer program FLUO [22]. The main results for the XAS data as x increases are a shift of the leading part of the O K edge to lower energy and an increase in absorption. As has been noted previously [23] and in our theory results below, the weak core-hole interaction at the O K edge means that the XAS closely follows the shape of the O-projected density of states. This allows us to make a direct connection with the evolution of electronic structure.

The magnetic state on O is probed by XMCD ($\mu^+ - \mu^-$, where μ^+ and μ^- are the absorption coefficients for $\pm$ circularly polarized x-rays with the sample in a B field high enough that the magnetization is close to saturation) as shown in the lower part of Fig. 2. A significant signal is only observed over a short energy range (~ 2 eV) at the beginning of the O K edge, indicating a nonzero orbital moment on the O site [24]. The amplitude of the XMCD signal increases with x and is surprisingly large above $x = 0.19$ compared to measurements of O XMCD in other systems; the formation of the FM metallic state appears to arise from the decreasing rhombohedral distortion with x.

To visualize how the electronic structure evolves with x, the Sr-induced change in XAS defined as XAS(x) − XAS($x = 0$) is shown in the top of Fig. 2. Sr induces a strong increase in the absorption at lower energy due to the formation of additional unoccupied oxygen ligand hole states. For low x, this new XAS peak shifts to lower energies and increases in amplitude as x increases, with no other changes in the XAS up to ~533 eV. For $x > 0.15$, there is no further shift, but the amplitude continues to increase with x and the XAS difference becomes negative above 529 eV [i.e., the O DOS decreases from 529–532 eV above the metal-insulator transition (MIT)]. The shaded regions in Figs. 1 and 2 illustrate that the energy range for which the XMCD is observed corresponds to the same energy range over which the additional peak in the XAS develops.

This increase in empty O DOS is consistent with Sr doping adding holes to the hybridized O bands. Note, however, that the density of oxygen states with quenched angular momentum (i.e. above 529 eV) decreases with x for x above ~0.18 eV. The induced O magnetic holes (DOS integral from 526–529 eV) and nonmagnetic holes (from 529–532 eV) are shown in Fig. 3. There is a clear change in these integrals near $x = 0.18$, where the MIT occurs and the system changes from a spin glass to a FM state.

To understand this evolution, we utilize doping-dependent electronic structure calculations. Recent studies suggest that a first principles density functional approach from an itinerant electron viewpoint can provide insights about the behavior of LSCO [25–27]. This is a

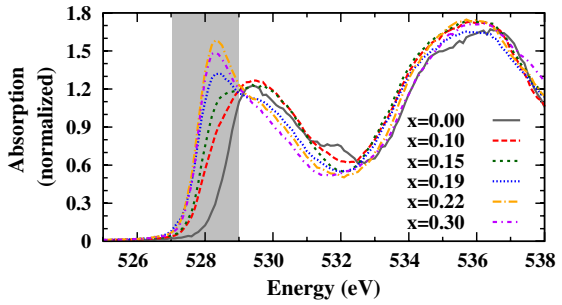

FIG. 1 (color online). XAS at the O K edge. The XAS data were normalized at 550 eV and self-absorption corrections were applied. The data agree well, except at the beginning of the edge (from 527–529 eV) where, with increasing x, a large increase in the XAS is observed, corresponding to the addition of empty states.

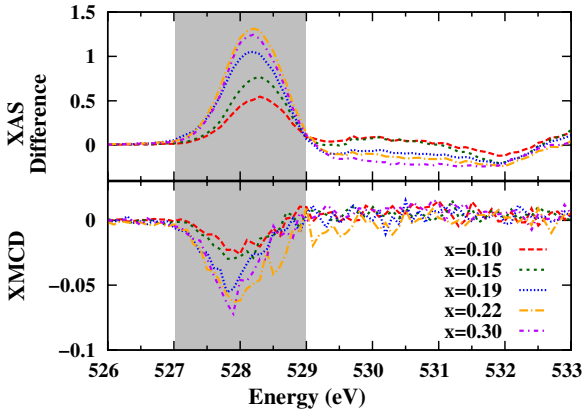

FIG. 2 (color online). Difference in the XAS (top) and XMCD (bottom) at the O K edge. A significant XMCD signal is only observed over this same small energy range (shaded region) where change in the XAS occurs and XAS(x) − XAS(0) is positive. Above 529 eV, the differences become slightly negative.

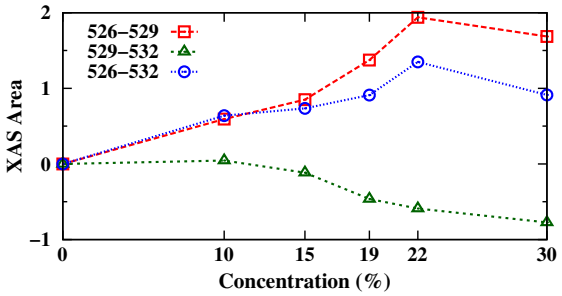

FIG. 3 (color online). Integrals of the difference in O XAS (Fig. 2) from 526–529 eV (magnetic holes) and from 529–532.5 eV (nonmagnetic holes) as a function of x; note that the change is not linear. For $x \leq 0.15$, the new magnetic holes are associated with FM clusters; over the range 0.15–0.22 where the material becomes fully FM, higher energy holes with no orbital momentum are converted to lower energy magnetic states.

homogeneous approach, which is typically applicable for itinerant or free-electron systems. We use the electronic states obtained from first principles band structure calculations to calculate theoretical XAS and XMCD spectra. For the electronic structure, we use a full-potential linearized augmented plane-wave (FPLAPW) method [28] with a local density functional [29,30]. We used $R_{\mathrm{MT}}K_{\mathrm{max}} = 8.0$ and $R_{\mathrm{MT}} = 2.2$, 2.2, 1.9, and 1.6 a.u. for La, Sr, Co, and O, respectively.

Because of the strong short range electronic interactions, the virtual crystal approximation (VCA) is not appropriate. Consequently, we use a $2 \times 2 \times 2$ supercell formed of eight pseudocubic unit cells, with Sr concentrations 0, 0.125, 0.25, and 0.375 as shown in Fig. 4. We initially kept the cubic structure even for the lower concentrations, since preliminary calculations indicated that the spectral features were more sensitive to the local atomic arrangement compared to the overall cell geometry. For the supercells, 40 k points were used for the iterations to self-consistency.

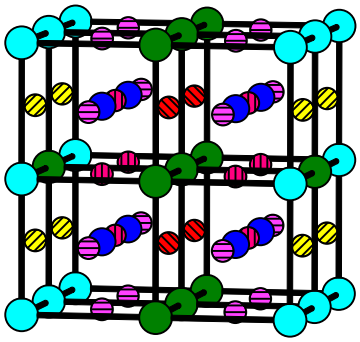

FIG. 4 (color online). $2 \times 2 \times 2$ supercell for a Sr doping of 3/8. Sr (large, light blue); La (large, dark green); Co (medium, blue). Four types of (small) O atoms with varying Sr neighbors: 0 (red, left slant); 1 (magenta, vertical); 2 (pink, horizontal); 3 (yellow, right slant).

The strong interactions between O $2p$ and Co $3d$ (particularly e_g) orbitals form well-separated bonding (-6 eV) and antibonding (-1 to 4 eV) states; see the orbital decomposed DOS in Fig. 5. A local model with e_g mainly above the t_{2g} states is inconsistent with these DOS. The generalized gradient approximation (GGA) and local density approximation (LDA) density functionals yield very similar DOS and only the LDA results are plotted. Our calculations for undoped $LaCoO_3$ are essentially in agreement with those of Ravindran *et al.* [26,27]. However, although the GGA [30] is more sensitive to the electronic correlations and yields a nonmagnetic ground state with experimental rhombohedral distortion (Co-O-Co bonding angle is 163.4°), LDA needs stronger distortion (Co-O-Co bonding angle is 158.4°) to yield the nonmagnetic state. The transition from the nonmagnetic to magnetic ground state (with $\sim 1.3\,\mu_B$ moments on Co) is not unlike the traditional local transition state picture, in the sense that about one Co d electron is promoted from spin-down to spin-up with very little cost in energy, and is very sensitive to the rhombohedral distortion. Using the experimental value for the rhombohedral distortion, the GGA calculation shows a ~ 3.2 meV/Co total energy difference between nonmagnetic and magnetic states.

We also extracted the theoretical O K edge [mainly a measure of the oxygen partial DOS (PDOS)] and the O XMCD signal, both as a function of x, as seen in Fig. 6. These theoretical results agree quite well with the experimental results shown in Figs. 1 and 2, though it is important to keep in mind that the energies are relative to E_F, so the XAS does not shift to lower energy as is observed experimentally, but the increases are quite similar and, again, we see there is only a large XMCD signal over the same

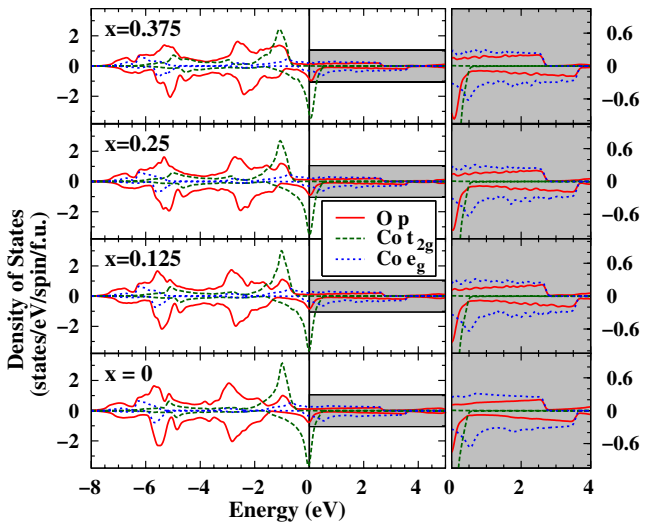

FIG. 5 (color online). Orbitally decomposed DOS for Co $3d$ (t_{2g} and e_g) and O $2p$ states from LDA calculations. For each panel top is spin-up, bottom, spin-down. The shaded region for $E \geq E_F$ is expanded on right.

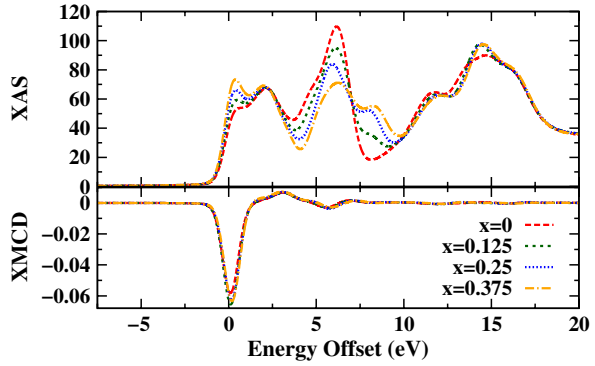

FIG. 6 (color online). Theoretical O K edge (top), showing a significant increase at the beginning of the edge, and calculated O K edge XMCD signal (bottom).

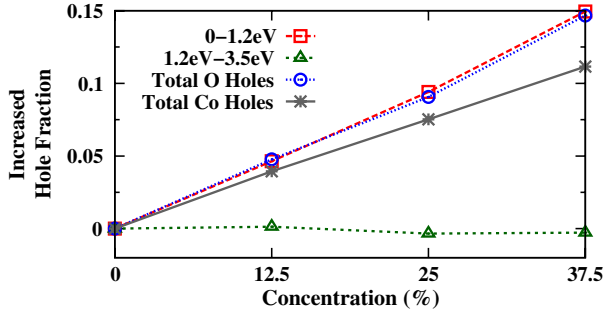

FIG. 7 (color online). Calculated hole fractions: magnetic O-hole fraction (red square), nonmagnetic O-hole fraction (green triangle), total O holes (blue circle), total Co holes (gray star).

energies for which the XAS has a large increase. The lack of an amplitude change with x is likely because the rhombohedral distortion was not included for small x.

Further important details are obtained by calculating the Sr-induced hole fraction on Co and O atoms, using similar energy ranges as for Fig. 3. In Fig. 7, we plot the induced hole density as a function of x; the calculated O hole density is comparable to but slightly larger than that on the Co atoms. Thus, surprisingly the induced holes are nearly equally distributed over the Co and O atoms, in good agreement with the experimental findings.

The calculations of the individual O magnetic moments are even more unusual and show that the O atoms in the supercell are not equivalent. Their properties depend on the number of neighboring Sr atoms, which can vary within the supercell (from 0 to up to 3 for $x = 0.375$): the larger the number of Sr neighbors, the larger the calculated magnetic moment (from $0.067\mu_B$ for O with 0 Sr neighbors to $0.121\mu_B$ for those with 3). Thus, these calculations show the limitations of the VCA; the system is not homogeneous at the local level. A similar situation occurs for Co, showing different Co moments on different sites, when calculated using a trigonal distortion of the basic unit cell, since the cubic $2 \times 2 \times 2$ supercell is too small to discriminate between different Co. Another interesting feature from the calculated O PDOS (Fig. 5) is that it provides a simple explanation as to why there are magnetic and nonmagnetic holes; just above E_F the spin-up and spin-down O PDOS are not equal so those energy states will have a net moment. At higher energies, the spin-up and down O PDOS are nearly equal and will have little moment.

In summary, we find that it is better to view these cobaltites in terms of bonding and antibonding states rather than split t_{2g} and e_g states. Some of the e_g symmetry states form bonding states and are filled; consequently, there is never the situation where some e_g are empty. A mixture of filled e_g and t_{2g} states may explain the wide range of conflicting experimental results about the Co spin state. Further, the broad range of the e_g DOS precludes a Jahn-Teller (J-T) interaction from being important. This likely explains the lack of a significant J-T distortion for the Co-O bonds [11,12].

The experimental changes in the O XAS and XMCD are not linear with x and appear to be correlated with the overall magnetism in the system, which changes from glasslike with FM clusters below 18% to metallic FM above 18%. Calculations qualitatively agree quite well with both the XAS and XMCD at the O K edge, and indeed find a small but significant spin magnetic moment on O atoms. Further, the theoretical results show that the properties of the O atoms are not all equivalent, and have different moments, confirming that the VCA is not adequate for describing systems such as LSCO, for which the electron density and oxygen moments are sensitive to nearby Sr positions. With part of the doped holes being on the O atoms, the Co-O Coulomb attraction that usually contributes to a shorter metal-O bond when holes are added is reduced and likely is a major reason as to why there is so little change in the Co-O bond length with doping.

The XAS and XMCD measurements were carried out at the Advanced Photon Source at Argonne National Laboratory and is supported by the U.S. Department of Energy, Office of Science under Grant No. DE-AC02-06CH11357. Work at the Ames Laboratory was supported by the U.S. Department of Energy, Basic Energy Sciences under Grant No. DE-AC02-07CH11358.

Note added in proof.—A recent explosive high field measurement up to 500 T on single crystal $LaCoO_3$ indicated a magnetic state appearing above 140 T with a magnetic moment of $\sim 1.4\ \mu_B$, which could correspond to the excited state with the same moment obtained by our band structure calculations [31].

[1] M. Imada, A. Fujimori, and Y. Tokura, Rev. Mod. Phys. **70**, 1039 (1998).
[2] J. Goodenough, Rep. Prog. Phys. **67**, 1915 (2004).

[3] M. Itoh, I. Natori, S. Kubota, and K. Motoya, J. Phys. Soc. Jpn. **63**, 1486 (1994).
[4] P. S. Anil Kumar, P. A. Joy, and S. K. Date, J. Phys. Condens. Matter **10**, L487 (1998).
[5] V. V. Sikolenko, A. P. Sazonov, I. O. Troyanchuk, D. Tobbens, U. Zimmermann, E. V. Pomjakushina, and H. Szymczak, J. Phys. Condens. Matter **16**, 7313 (2004).
[6] H. M. Aarbogh, J. Wu, L. Wang, H. Zheng, J. F. Mitchell, and C. Leighton, Phys. Rev. B **74**, 134408 (2006).
[7] C. He, M. A. Torija, J. Wu, J. W. Lynn, H. Zheng, J. F. Mitchell, and C. Leighton, Phys. Rev. B **76**, 014401 (2007).
[8] M. Kriener, M. Braden, H. Kierspel, D. Senff, O. Zabara, C. Zobel, and T. Lorenz, Phys. Rev. B **79**, 224104 (2009).
[9] S. Yamaguchi, Y. Okimoto, H. Taniguchi, and Y. Tokura, Phys. Rev. B **53**, R2926 (1996).
[10] K. Knížek, P. Novák, and Z. Jirák, Phys. Rev. B **71**, 054420 (2005).
[11] N. Sundaram, Y. Jiang, I. E. Anderson, D. P. Belanger, C. H. Booth, F. Bridges, J. F. Mitchell, T. Proffen, and H. Zheng, Phys. Rev. Lett. **102**, 026401 (2009).
[12] Y. Jiang, F. Bridges, N. Sundaram, D. P. Belanger, I. E. Anderson, J. F. Mitchell, and H. Zheng, Phys. Rev. B **80**, 144423 (2009).
[13] M. Sikora, C. Kapusta, K. Knizek, Z. Jirak, C. Autret, M. Borowiec, C. J. Oates, V. Prochazka, D. Rybicki, and D. Zajac, Phys. Rev. B **73**, 094426 (2006).
[14] A. R. Han, S. Hwang, Y. Zhao, and Y. Kwon, J. Magn. Magn. Mater. **320**, 1591 (2008).
[15] F. Bridges, C. H. Booth, M. Anderson, G. H. Kwei, J. J. Neumeier, J. Snyder, J. Mitchell, J. S. Gardner, and E. Brosha, Phys. Rev. B **63**, 214405 (2001).
[16] R. Caciuffo, D. Rinaldi, G. Barucca, J. Mira, J. Rivas, M. A. Senaris-Rodriguez, P. G. Radaelli, D. Fiorani, and J. B. Goodenough, Phys. Rev. B **59**, 1068 (1999).
[17] A. Mineshige, M. Kobune, S. Fujii, Z. Ogumi, M. Inaba, T. Yao, and K. Kikuchi, J. Solid State Chem. **142**, 374 (1999).
[18] T. Saitoh, T. Mizokawa, A. Fujimori, M. Abbate, Y. Takeda, and M. Takano, Phys. Rev. B **56**, 1290 (1997).
[19] O. Toulemonde, N. N'Guyen, and F. S. A. Traverse, J. Solid State Chem. **158**, 208 (2001).
[20] J. Okamoto *et al.*, Phys. Rev. B **62**, 4455 (2000).
[21] M. Merz, P. Nagel, C. Pinta, A. Samartsev, H. v. Löhneysen, M. Wissinger, S. Uebe, A. Assmann, D. Fuchs, and S. Schuppler, Phys. Rev. B **82**, 174416 (2010).
[22] D. Haskel, FLUO: correcting XANES for self-absorption in fluorescence data, http://www.aps.anl.gov/~haskel/fluo.html.
[23] D. D. Sarma, N. Shanthi, and P. Mahadevan, Phys. Rev. B **54**, 1622 (1996).
[24] J.-I. Igarashi and K. Hirai, Phys. Rev. B **50**, 17820 (1994).
[25] H. Takahashi, F. Munakata, and M. Yamanaka, Phys. Rev. B **57**, 15211 (1998).
[26] P. Ravindran, P. A. Korzhavyi, H. Fjellvag, and A. Kjekshus, Phys. Rev. B **60**, 16423 (1999).
[27] P. Ravindran, H. Fjellvåg, A. Kjekshus, P. Blaha, K. Schwarz, and J. Luitz, J. Appl. Phys. **91**, 291 (2002).
[28] P. Blaha, K. Schwarz, G. K. H. Madsen, D. Kvasnicka, and J. Luitz, *WIEN2k, An Augmented Plane Wave + Local Orbitals Program for Calculating Crystal Properties* (Karlheinz Schwarz, Technische Universität Wien, Austria, 2001).
[29] J. P. Perdew and Y. Wang, Phys. Rev. B **45**, 13244 (1992).
[30] J. P. Perdew, K. Burke, and M. Ernzerhof, Phys. Rev. Lett. **77**, 3865 (1996).
[31] V. V. Platonov, Yu. B. Kudasov, M. P. Monakhov, and O. M. Tatsenko, Phys. Solid State, **54**, 279 (2012).